

Transfer Learning Bayesian Optimization to Design Competitor DNA Molecules for Use in Diagnostic Assays

Ruby Sedgwick^{1,2}, John P. Goertz¹, Molly M. Stevens^{1,3}, Ruth Misener², and Mark van der Wilk²

¹Department of Materials, Department of Bioengineering and Institute of Biomedical Engineering, Imperial College London, London

²Department of Computing, Imperial College London, London

³Department of Physiology, Anatomy and Genetics, Department of Engineering Science, and Kavli Institute for Nanoscience Discovery, University of Oxford, Oxford

February 28, 2024

Abstract

With the rise in engineered biomolecular devices, there is an increased need for tailor-made biological sequences. Often, many similar biological sequences need to be made for a specific application meaning numerous, sometimes prohibitively expensive, lab experiments are necessary for their optimization. This paper presents a transfer learning design of experiments workflow to make this development feasible. By combining a transfer learning surrogate model with Bayesian optimization, we show how the total number of experiments can be reduced by sharing information between optimization tasks. We demonstrate the reduction in the number of experiments using data from the development of DNA competitors for use in an amplification-based diagnostic assay. We use cross-validation to compare the predictive accuracy of different transfer learning models, and then compare the performance of the models for both single objective and penalized optimization tasks.

1 Introduction

Tailoring biological sequences, such as oligonucleotides or proteins, for specific applications is a common challenge in bioengineering. These engineered molecules have a variety of uses including in biosensors (Hua et al., 2022; Deng et al., 2023; Goertz et al., 2023), medical therapeutics (Badeau et al., 2018; Blakney et al., 2019; Ebrahimi and Samanta, 2023) and bio-computing (Siuti et al., 2013; Qian et al., 2011; Lv et al., 2021). However, development often requires expensive or time consuming experiments, meaning good experimental design is necessary to optimize the biological sequences within the experimental budget (Cox and Reid, 2000). This also leads to better analysis, especially when there are interaction effects between input factors, which is common in biological experiments (Kreutz and Timmer, 2009; Politis et al., 2017; Papanephytous, 2019; Fellermann et al., 2019; Narayanan et al., 2020; Gilman et al., 2021).

Iterative experimental designs have the advantage of using information from previous experiments to inform future ones. Bayesian optimization is an iterative global black-box optimization strategy (Snoek et al., 2012; Shahriari et al., 2016) which has proven effective for the design of biomolecular experiments including antibody development (Khan et al., 2023), extracellular vesicle production (Bader et al., 2023),

design and manufacturing of proteins and tissues (Romero et al., 2013; Mehrian et al., 2018; Narayanan et al., 2021; Gamble et al., 2021), validation of molecular networks (Sedgwick et al., 2020) and vaccine production (Rosa et al., 2022). In Bayesian optimization, a surrogate model, usually a Gaussian process, of the system is built using data and an acquisition function decides which data point to collect next. Gaussian processes are a powerful tool for designing biological experiments in low data regimes due to their uncertainty estimates (Hie et al., 2020).

When many similar biological sequences need to be designed, it can be even harder to optimize all the sequences within the experimental budget. Optimizing each sequence from scratch discards useful information from previous tasks, meaning more experiments are required. An alternative is to use transfer learning — a technique that improves the learning of new sequences by sharing information between optimization tasks (Zhuang et al., 2021).

As we require our surrogate model to be data efficient and have uncertainty quantification, we consider four transfer learning Gaussian process models: an average Gaussian process (AvgGP), the multi-output Gaussian process (MOGP), the linear model of coregionalisation (LMC) and the latent variable multi-output Gaussian process (LVMOGP). The key difference between these Gaussian process models lies in their handling of correlations between outputs: from no correlation in the MOGP to non-linear correlation in the LVMOGP.

We apply these surrogate model in conjunction with Bayesian optimization for efficient optimization of bio-molecules, as shown in Figure 1. We focus specifically on the development of a new modular diagnostic assay, based on competitive polymerase chain reaction (PCR), for measuring expression of multiple genes simultaneously, giving a single end point readout (Goertz et al., 2023). This diagnostic requires many competitor DNA sequences to be optimized to have the correct amplification properties in PCR reactions, and we believe the relationship between the responses of the competitors may be non-linear. For optimal results, these competitors should have a predefined amplification curve rate; and a nuisance drift factor should ideally be below a certain threshold to allow for a more stable readout.

We use synthetic data experiments to compare transfer learning Gaussian process models in different settings. We then use cross-validation to verify the benefit of the LVMOGP for modeling the response of the competitors, using data from DNA amplification experiments. We confirm that a LVMOGP surrogate model in conjunction with the design of experiments workflow speeds up optimization of the competitors for both a single objective case, where only rate is optimized, and an optimization case with a penalty on drift over a given threshold.

2 Materials and Methods

2.1 Gaussian Process Regression

A Gaussian process is a stochastic process representing an infinite collection of random variables, the joint distribution of any subset of which is a multi-dimensional Gaussian distribution (Rasmussen and Williams, 2006). A Gaussian process is fully defined by its mean $m : \mathbb{R}^D \mapsto \mathbb{R}$ and covariance $k : \mathbb{R}^D \times \mathbb{R}^D \mapsto \mathbb{R}$ functions:

$$f(\mathbf{x}) \sim \mathcal{GP}(m(\mathbf{x}), k(\mathbf{x}, \mathbf{x}')), \quad (1)$$

where $\mathbf{x} \in \mathbb{R}^D$. For a full nomenclature see Appendix 8. The output data $y(\mathbf{x}) \in \mathbb{R}$ is assumed to be noisy evaluations of $f(\mathbf{x}) \in \mathbb{R}$:

$$y(\mathbf{x}) = f(\mathbf{x}) + \epsilon, \quad (2)$$

where $\epsilon \sim \mathcal{N}(0, \sigma_n^2)$ and σ_n^2 is the noise variance.

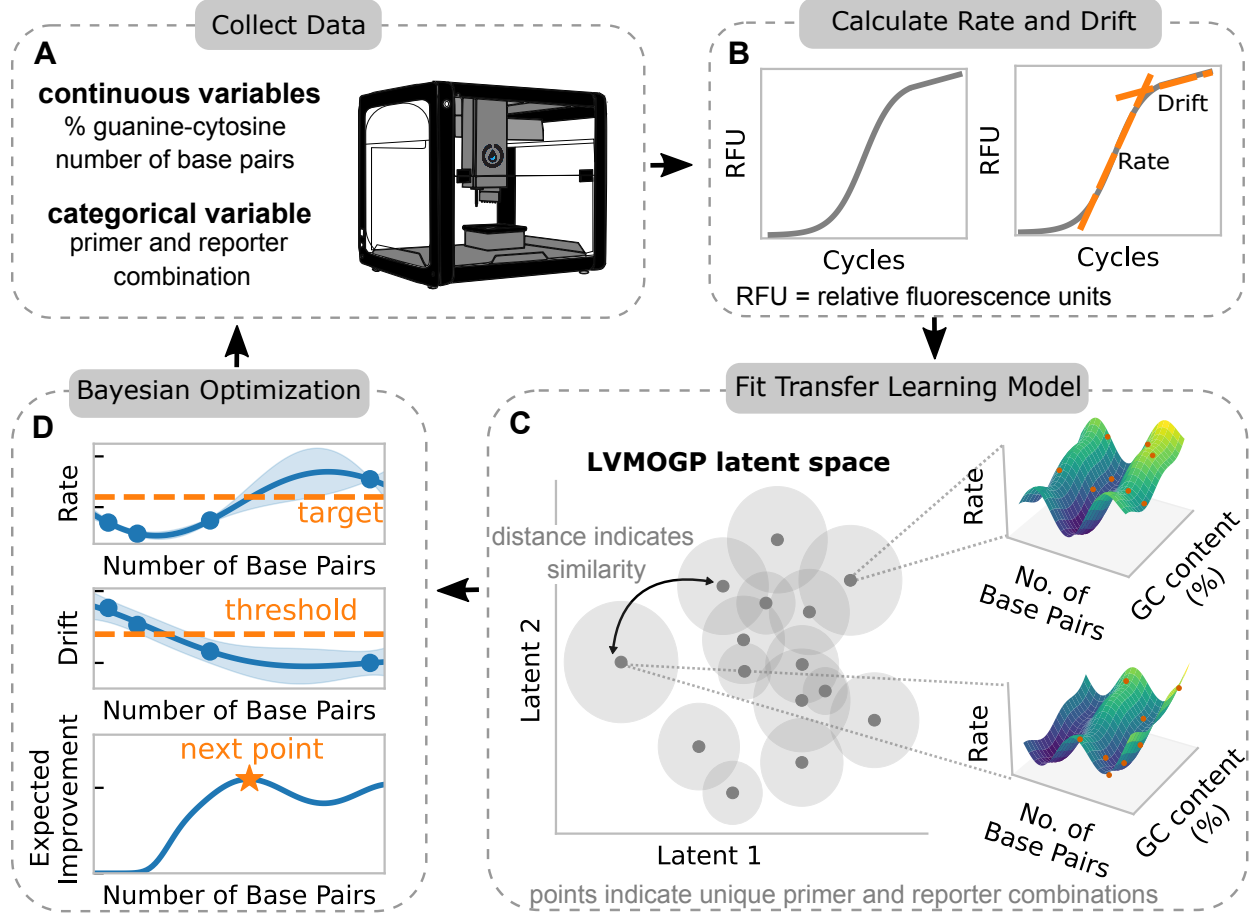


Figure 1: Design of experiments workflow for optimizing the competitor DNA molecules. **(A)** Data is collected in the lab using a DNA amplification reaction assay. **(B)** The rate and drift are then calculated by fitting them to the amplification curves. **(C)** Transfer learning surrogate models use the data to predict the rate and drift for each of the given competitors. **(D)** A Bayesian optimization algorithm selects the experiment to run for each competitor. This process is repeated until all optimal competitor sequences are found or the experimental budget is exhausted.

Prior beliefs about the data can be expressed in the selection of the mean and covariance functions. Often this implies setting the mean function to zero, which is what we do here. A common kernel function is the squared exponential, which is a stationary kernel that assumes the data-generating function is smooth:

$$k(\mathbf{x}, \mathbf{x}') = \sigma_k^2 \exp \left(- \sum_{d=1}^D \frac{(x_d - x'_d)^2}{2\ell_d^2} \right), \quad (3)$$

where σ_k^2 is the kernel variance and ℓ_d is the lengthscale of dimension d . Given a set of N training data $\mathcal{D} = \{(\mathbf{x}_i, y_i) | i = 1, \dots, N\}$, the training inputs $\{\mathbf{x}_i\}_{i=1}^N$ can be aggregated into the matrix $\mathbf{X} \in \mathbb{R}^{N \times D}$ and the training observations $\{y_i\}_{i=1}^N$ aggregated into the vector $\mathbf{y} \in \mathbb{R}^N$. It is then possible to write a joint distribution of the training observations \mathbf{y} and predicted function value \mathbf{f}_* at prediction locations \mathbf{X}_* . Thus, the mean and covariance of the Gaussian process at the prediction points can be calculated respectively:

$$\mu(\mathbf{X}_*) = \mathbb{E}[\bar{\mathbf{f}}_* | \mathbf{X}, \mathbf{y}, \mathbf{X}_*] = \mathbf{K}(\mathbf{X}_*, \mathbf{X}) [\mathbf{K}(\mathbf{X}, \mathbf{X}) + \sigma_n^2 \mathbf{I}]^{-1} \mathbf{y} \quad (4)$$

$$\sigma(X_*) = K(X_*, X_*) - K(X_*, X)[K(X, X) + \sigma_n^2 \mathbf{I}]^{-1} K(X, X_*). \quad (5)$$

The hyperparameters $\theta = \{\sigma_n^2, \sigma_k^2, \ell_d\}$ are optimized by maximizing the marginal likelihood $p(\mathbf{y}|X, \theta)$, which is calculated in closed form (Rasmussen and Williams, 2006).

2.2 Transfer Learning Gaussian Processes

2.2.1 Independent Gaussian Processes with Shared Kernel

A simple way of transferring information is through the kernel hyperparameters. In the multi-output Gaussian process (MOGP), the outputs are assumed to be multi-dimensional such that $\mathbf{y} \in \mathbb{R}^{N \times P}$ (Álvarez et al., 2012). All outputs have the same kernel function and hyperparameters but function values on different outputs are uncorrelated. This means the kernel of the MOGP is a block diagonal with $k(X_p, X'_p) = k(X_p, X'_p)$ if $p = p'$ and $k(X_p, X'_p) = 0$ if $p \neq p'$ where p is the output index. The joint distribution for two outputs \mathbf{f}_1 and \mathbf{f}_2 evaluated at points X_1 and X_2 is given by:

$$\begin{bmatrix} \mathbf{f}_1 \\ \mathbf{f}_2 \end{bmatrix} \sim \mathcal{N} \left(\mathbf{0}, \begin{bmatrix} K(X_1, X_1) & \mathbf{0} \\ \mathbf{0} & K(X_2, X_2) \end{bmatrix} \right). \quad (6)$$

2.2.2 Linear Model of Coregionalization

The linear model of coregionalization (LMC) extends the MOGP to model linear correlations between output surfaces by assuming they are linear combinations of Gaussian process latent functions:

$$f_p(\mathbf{x}) = \mathbf{W}_p g(\mathbf{x}) + \kappa_p v_p(\mathbf{x}). \quad (7)$$

where $\mathbf{W} \in \mathbb{R}^{P \times Q}$ is a vector of weights $g(\mathbf{x}) = \{g_q(\mathbf{x})\}_{q=1}^Q$ are shared latent functions, $v_p(\mathbf{x})$ is a latent function that shares the kernel of $g(\mathbf{x})$ and allows for some independent behavior and κ_p is a learned constant (Álvarez et al., 2012; Bonilla et al., 2007).

This leads to a kernel structured in such a way that the joint distribution between two functions \mathbf{f}_1 and \mathbf{f}_2 is given by:

$$\begin{bmatrix} \mathbf{f}_1 \\ \mathbf{f}_2 \end{bmatrix} \sim \mathcal{N} \left(\mathbf{0}, \begin{bmatrix} \sum_{q=1}^Q b_{11} k_q(X_1, X_1) & \sum_{q=1}^Q b_{12} k_q(X_2, X_2) \\ \sum_{q=1}^Q b_{21} k_q(X_1, X_1) & \sum_{q=1}^Q b_{22} k_q(X_2, X_2) \end{bmatrix} \right), \quad (8)$$

where $b_{pp'}$ is an element of $B = \mathbf{W}\mathbf{W}^T + \text{diag}(\boldsymbol{\kappa})$, a $P \times P$ matrix determining the similarity between functions and there are Q different covariance functions $k_q(\mathbf{x}, \mathbf{x}')$. If $Q = 1$, this is known as the intrinsic coregionalization model (Álvarez et al., 2012).

Coregionalization methods have successfully been used for Bayesian optimization (Cao et al., 2010; Swersky et al., 2013; Tighineanu et al., 2022) and applied to the optimization of synthetic genes (González et al., 2015) and chemical reactions (Taylor et al., 2023). However, coregionalization methods assume the response surfaces are linear combinations of a small number of latent functions, so they can fail to fit and predict well on data with non-linear similarity between surfaces.

2.2.3 Latent Variable Multi-output Gaussian Process

The latent variable multi-output Gaussian process (LVMOGP) introduced by Dai et al. (2017) can model non-linear similarities. It does so by augmenting the input domain of a Gaussian process with a Q_H dimensional latent space \mathcal{H} . Each output function has a latent variable, such that the latent variables are denoted by $H = [\mathbf{h}_1, \dots, \mathbf{h}_P]^T \in \mathbb{R}^{P \times Q_H}$. The LVMOGP assumes output \mathbf{y}_p is generated by:

$$y_p(\mathbf{x}) = f(\mathbf{x}, \mathbf{h}_p) + \epsilon, \quad (9)$$

where $\epsilon \sim \mathcal{N}(0, \sigma_n^2)$. The latent space allows the LVMOGP to automatically transfer learn between output functions as it will cluster similar output functions together and place widely different ones far apart on the latent space. The distance on the latent space and the latent space lengthscale then determine the amount of correlation between different output functions. To account for uncertainty in the placement of the latent variables, they are treated as distributions rather than point estimates, such that $\mathbf{h}_p \sim \mathcal{N}(\mu_{h_p}, \Sigma_{h_p})$. For more details on the implementation of the LVMOGP see Appendix 8.1.

Similar latent variable models have been used for Bayesian optimization of material development (Zhang et al., 2020) and for transfer learning across cell lines (Hutter et al., 2021). However, these methods treat the latent variables as point estimates rather than distributions as in the LVMOGP, which can cause poor uncertainty estimates, especially at low data regimes.

2.2.4 Comparison of Gaussian Process Models

In our comparisons, we include a fourth model called the average Gaussian process (AvgGP), which treats all the data as if it has come from the same response surface. Figure 2 shows predictions on a toy data set of the four Gaussian process models we consider. As the AvgGP doesn't differentiate between surfaces, it doesn't fit any response surface well. The MOGP only shares hyperparameters but no information about function values between response surfaces, meaning it makes worse predictions and has more uncertainty on new response surfaces. The LMC has a better mean prediction than the MOGP as it shares information between response surfaces. The LVMOGP similarly has better mean prediction than the MOGP as it shares information across response surfaces through the latent space. If $Q = 1$ and B is the identity matrix, then the LMC recovers the MOGP. If a linear kernel is applied to the latent dimensions of the LVMOGP, the LMC is recovered, and by making the distance between latent variables large relative to the lengthscale, the MOGP can be recovered too. The fact there are hyperparameter settings for the LMC and LVMOGP that recover the MOGP is promising for preventing negative transfer, as in the case where there is no correlation between response surfaces they can just revert to the MOGP. However, this is only true for large data sets — in low data regimes, we may expect some negative transfer in the no correlation case, due to uncertainty in the hyperparameter values and, in the case of the LVMOGP, a prior on the existence of correlations.

2.2.5 Gaussian Process Implementation

All coding was done in Python using version 3.9. The Gaussian process models were implemented using GPFlow 2.3.0 (Matthews et al., 2017). GPFlow has implementations of the standard Gaussian process, MOGP and the LMC. Our LVMOGP was implemented as a new GPflow model class, which can be accessed via the Github links in Appendix 8.2. Other packages used include PyMC3 3.11.4 (Salvatier et al., 2016) for Bayesian parameter estimation, Numpy 1.21.4 (Harris et al., 2020), Scipy 1.7.1 (Virtanen et al., 2020) and Pandas 1.3.4 (The pandas development team, 2023) for data processing and Matplotlib 3.4.3 (Droettboom et al., 2015) for visualization.

2.3 Bayesian Optimization

Bayesian optimization is a sequential experimental design strategy for finding the global minimum (or maximum) of an objective function (Shahriari et al., 2016; Snoek et al., 2012). As the objective function is unknown, a surrogate model is used to represent the posterior belief of the objective function and updated every time a new data point is observed. An acquisition function is then used to select the next data point to collect. A common acquisition function is the expected improvement which trades off exploration of regions with little data and exploitation of regions which are expected to be optimal

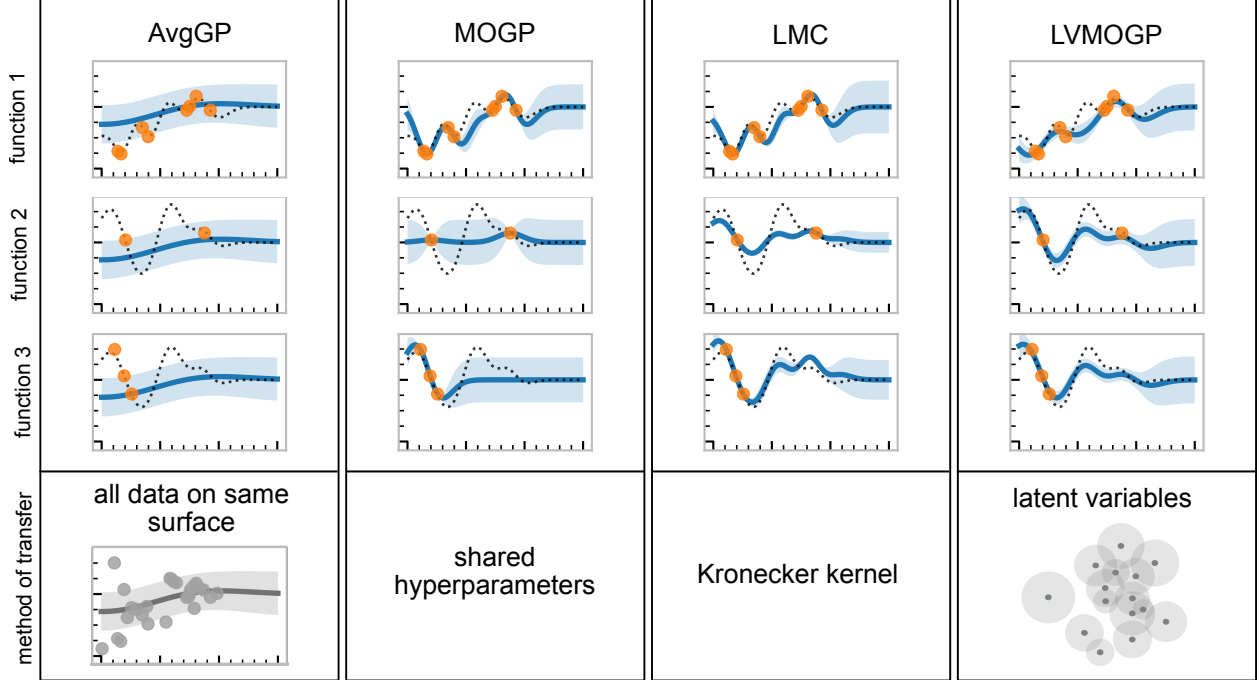


Figure 2: Predictions of the four Gaussian process models fitted to a toy dataset. MOGP: multioutput Gaussian process, AvgGP: average Gaussian process, LMC: linear model of coregionalization, LVMOGP: latent variable multi-output Gaussian process. The dots are the data, the dashed line is the true function, the solid line is the Gaussian process mean prediction and the shaded region is 2 times the predicted standard deviation, meaning around 95% of the data points should lie within the shaded region. The bottom row explains how data is transferred between the surfaces by each model.

(Jones et al., 1998; Garnett, 2023). This process is repeated until the optimum has been found or the experimental budget exhausted.

2.3.1 Acquisition Function

Rather than maximizing or minimizing the rate, as is usual in Bayesian optimization, we wish to minimize the difference between the rate, f_{rate} , and the target rate, T_{rate} :

$$\arg \min_{BP, GC} \sqrt{(f_{\text{rate}} - T_{\text{rate}})^2} \quad (10)$$

Therefore, we use the target vector optimization acquisition function, that extends the expected improvement acquisition function to minimize the Euclidean distance between a target vector and a vector of the current predicted values (Uhrenholt and Jensen, 2019). As we are only optimizing the rate, we use their formulation with scalars instead of vectors. In this formulation, a stochastic variable is defined as $\delta|\mathbf{x} = \|y(\mathbf{x}) - y^t\|_2^2$ where $y(\mathbf{x})$ is the output value at input \mathbf{x} and y^t is our target value. The distribution of $p(\delta|\mathbf{x})$ is modeled with the aim of minimizing δ . If the response surfaces are Gaussian processes, then $p(\delta|\mathbf{x})$ can be approximated using a non-central χ^2 distribution. The expected improvement for this non-central χ^2 distribution is expressed as:

$$\alpha_{EI} = \delta_{\min} G_{\lambda}(\delta_{\min}/\gamma^2) - \gamma^2 \mathbb{E}[t | t < \delta_{\min}/\gamma^2] G_{\lambda}(\delta_{\min}/\gamma^2), \quad (11)$$

where δ_{min} is the minimum δ observed so far, γ is root mean of the variances of each output evaluated at the training points, $t = \delta\gamma^{-2}$, and G_λ is an approximate cumulative χ^2 distribution with non-centrality parameter λ defined in the paper (Uhrenholt and Jensen, 2019).

2.3.2 Bayesian Optimization with Drift Penalty

To ensure the drift value remains below, or close to the threshold, we use the *probability of feasibility* to encourage the algorithm to select points that have a high chance of being below the threshold (Schonlau et al., 1998):

$$PF(\mathbf{x}) = p(f_{drift}(\mathbf{x}) \leq T_{drift}), \quad (12)$$

where $f_{drift}(\mathbf{x})$ is the value of drift function at \mathbf{x} , and T_{drift} is the drift threshold.

We then multiply the expected improvement by the probability of feasibility to get our final acquisition function:

$$\alpha_p = PF(\mathbf{x})\alpha_{EI}(\mathbf{x}). \quad (13)$$

The probability of feasibility has been used for optimization applications including analog circuits (Lyu et al., 2018) and materials design (Sharpe et al., 2018).

2.3.3 Performance Metrics

For both the synthetic experiments and the cross-validation experiments we assessed the fit of Gaussian process models with two performance metrics: root mean squared error (RMSE):

$$RMSE = \sqrt{\frac{\sum_{i=0}^{N^*} (\mu(\mathbf{x}_i^*) - y_i^*)^2}{N^*}}, \quad (14)$$

and negative log predictive density (NLPD):

$$NLPD = \frac{1}{N^*} \sum_{i=0}^{N^*} \log p(y_i^* | \mathbf{x}_i^*, X, \mathbf{y}, \boldsymbol{\theta}) = -\frac{1}{2N^*} \sum_{i=0}^{N^*} \left(-\log(2\pi\sigma(\mathbf{x}_i^*)^2) - \frac{(y_i^* - \mu(\mathbf{x}_i^*))^2}{\sigma(\mathbf{x}_i^*)^2} \right). \quad (15)$$

These are both calculated on a test set of input locations X^* of length N^* . The RMSE is useful for comparing the mean predictions of the Gaussian processes, while the NLPD also indicates how good the uncertainty estimate is, both of which are important for effective exploration and exploitation. For assessing the Bayesian optimization algorithm, we use cumulative regret:

$$\text{regret} = \min_{\mathbf{x}_i \in X} \left(\sqrt{(\mu(\mathbf{x}_i) - y_{best})^2} + \max(0, f_{drift}(\mathbf{x}_i) - T_{drift}) \right), \quad (16)$$

where y_{best} is the data point closest to the target out of both training and candidate sets for that surface. $\max(0, f_{drift}(\mathbf{x}_i) - T_{drift})$ is a penalty for exceeding the drift threshold.

2.4 Data Collection

Each competitor has predefined primers and fluorescent probes and a design region where the sequence can be altered. Rather than tackling the difficult combinatorial problem of optimizing the sequence directly, we reduce the problem to two key input variables: the number of base pairs (BP) and guanine-cytosine content (GC) as in Figure 3. This converts the design space into a more manageable continuous form and reduces the input dimensions, which is beneficial when data is limited. For each BP-GC

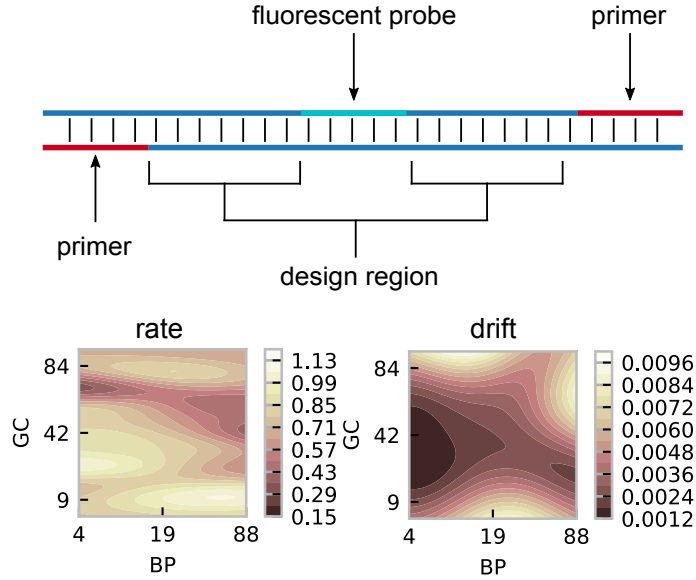


Figure 3: Schematic of the competitor design space. For a given competitor DNA molecule, the primers and fluorescent probe regions are fixed. We can edit the design region to ensure the sequence has a given number of base pairs and guanine-cytosine content. Changing the number of base pairs and guanine-cytosine-content affects the rate and drift of the competitor, allowing us to fine-tune to the rate and drift required for the diagnostic assay.

combination, chosen by an expert researcher, a polymerase chain reaction (PCR) assay generates an amplification curve, from which rate and drift are calculated. In total, we have data on 34 different competitors and wish to optimize 16 of these. Across the 34 competitors, we have 592 data points at 327 unique input locations, with 1 to 6 repeats at each location. See Appendix 8.3 for a summary of the data.

The rate and drift for each amplification curve were calculated using the following equations:

$$F_T = \frac{\nu}{1 + \frac{(\nu - F_0)}{F_0} \cdot e^{-r \cdot \tau}}, \quad (17)$$

$$\text{signal} = F_T \cdot \left(1 + \frac{F_T}{\nu} \cdot m \cdot (\ln(F_0)/r) \right), \quad (18)$$

where F_T and F_0 are the end point and starting fluorescence, ν is carrying capacity, r is the rate, m is the drift and τ is cycle number.

2.4.1 Polymerase Chain Reactions

To perform the PCR reactions, we used an Applied Biosystems QuantStudio 6 Flex using Applied Biosystems MicroAmp EnduraPlate Optical 384-well plates (Thermo Fisher Scientific, Waltham, MA, USA). The thermocycling stages consisted of a melt step at 95°C for 3 seconds and an annealing step at 60°C. All reactions were performed at 10 μ L and used Applied Biosystems TaqMan Fast Advanced Master Mix. Either fluorescent probes or EvaGreen dye (Biotium, Fremont, CA, USA) were used as reporters.

2.4.2 DNA Sequences

For each BP-GC combination for a given competitor, NUPACK (Zadeh et al., 2011) was used to create a DNA sequence with the correct number of base pairs and guanine-cytosine content, as well as the correct sequences for the primer and probes. These sequences, alongside synthetic natural target analogs, were purchased from Twist Biosciences (San Francisco, CA) or as eBlock Gene Fragments from Integrated DNA Technologies (“IDT”, Coralville, IA, USA). Primers and probes were also purchased from IDT.

3 Results

3.1 Synthetic Data Experiments

To explore the performance of the MOGP, AvgGP, LMC and LVMOGP, we ran experiments on synthetic data sets representing three test cases: uncorrelated, linearly correlated and horizontally offset response surfaces. All synthetic experiments had two response surfaces each with 30 points observed and 10 new response surfaces with no points observed initially. We added one random point to each new response surface every iteration and recorded the RMSE and NLPD for the Gaussian process models’ predictions. Figure 4 shows the RMSEs and NLPDs of the Gaussian process models for these test settings.

For the uncorrelated test case, response surfaces were generated as independent samples of a Gaussian process prior with a $\ell = 0.3$ and $\sigma_k^2 = 2$. This test case was to check for negative transfer, where the sharing of information hinders rather than aids the learning process. In Figure 4, the MOGP outperforms the other Gaussian process models for RMSE and NLPD until approximately 10 data points. We expect the LMC and LVMOGP to have some negative transfer at very low data regimes as they have a prior expectation of correlations between response surfaces. However, with enough data, they should perform the same as the MOGP, which is corroborated by the results in Figure 4.

The response surfaces for the linearly-correlated test case were created as linear combinations of two latent functions, both generated as independent samples of a Gaussian process with $\ell = 0.3$ and $\sigma_k^2 = 2$. The LMC outperforms the other two Gaussian process models except at very low data regimes, which is likely due to overconfidence of the LMC when it has little data. The LMC and LVMOGP outperform the MOGP even at high data regimes, showing the advantage of transfer learning.

The horizontally offset test case was chosen as a simple example where the LMC struggles to fit the data. The response surfaces were generated by offsetting a sigmoid function horizontally by a random constant. In this case, the LVMOGP outperforms the other Gaussian process models for both RMSE and NLPD. This is because the LVMOGP can learn new surfaces with very few data points, as all it needs to do is to correctly predict where the sloped region is. The LMC performs worse than the LVMOGP because the offset cannot be represented by a linear combination of its latent functions, meaning it requires more data to perform as well.

Across all the test cases, the LMC has poor NLPD at low data regimes. This is likely because it cannot express uncertainty in the deterministic B matrix.

3.2 Prediction of DNA Amplification Experiments

The performance of the proposed design of experiments workflow was validated using data from competitor DNA amplification experiments. This was done in three parts: first cross-validation was performed to compare the predictive accuracy of the Gaussian process models; then a Bayesian optimization procedure was used to optimize only the rate; finally the Bayesian optimization with drift penalty procedure was applied.

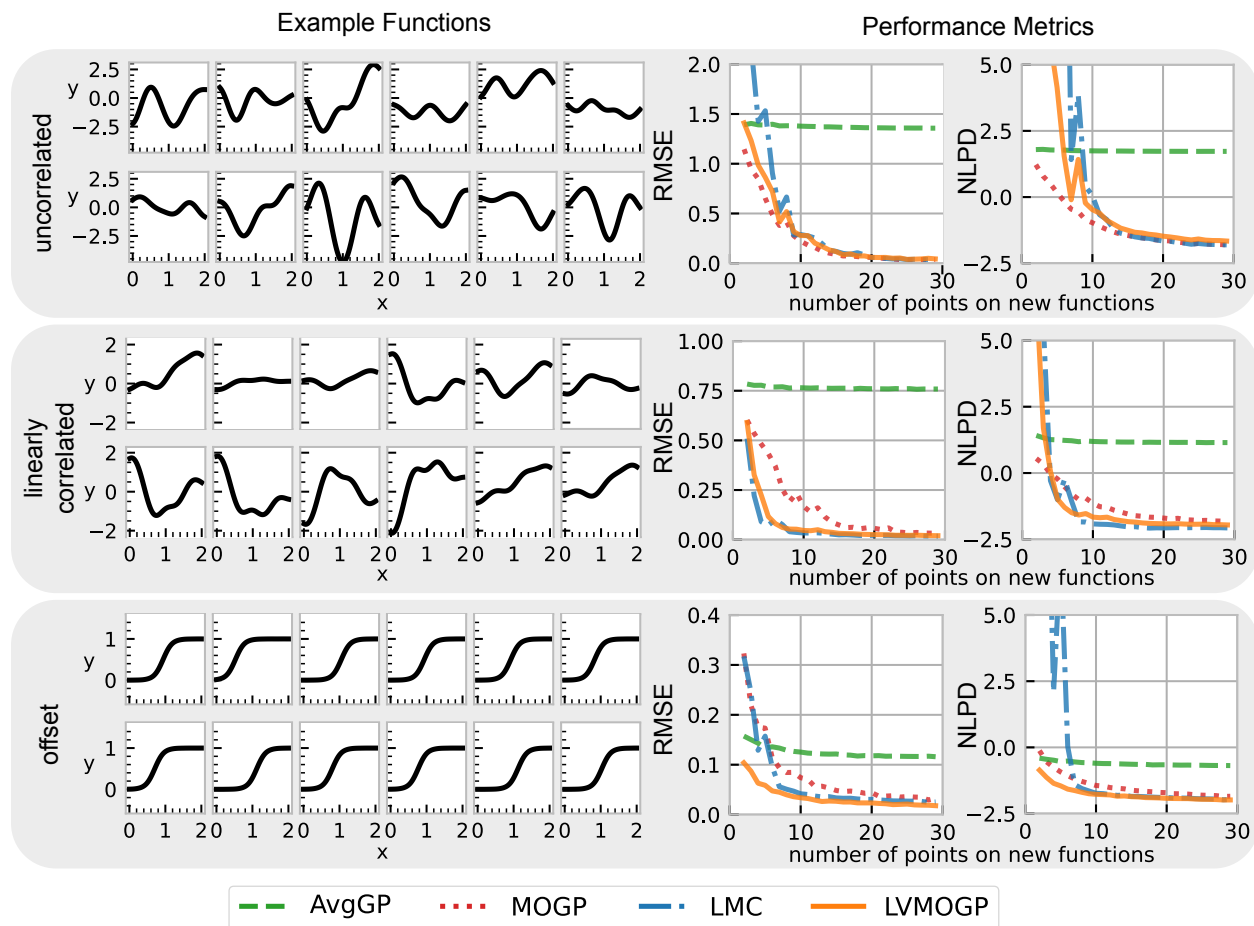


Figure 4: Results of experiments with synthetically-generated data. The plots on the left show example data-generating functions used for the synthetic experiments. The plots on the right show the RMSE and NLPD for the three different test response surface types for each of the Gaussian process models. New points are added randomly, and each line is the mean of 5 different randomly generated data sets, all generated from the same test functions.

In cross-validation, the training set consisted of all the data from the two competitors that had the most observations as well as a random subset of the remaining data, but ensuring all competitors had at least one data point. This was repeated 150 times for each percentage of data in the training set. Figure 5 shows the RMSE and NLPD of the Gaussian process models' predictions. The LVMOGP outperforms the other Gaussian process models for both RMSE and NLPD for both rate and drift. The LMC has poor NLPD in comparison to the other Gaussian process models, suggesting it has poor uncertainty estimates. The AvgGP model shows little improvement with increased amounts of training data. This shows the limitations of averaging the surfaces and justifies modeling each response surface separately.

3.3 Optimization of DNA Amplification Experiments

Ideally, for the Bayesian optimization experiments we would integrate the algorithm into the experimental loop, collecting new data with each new recommendation of each Gaussian process model. However, due to the cost of experiments, this was infeasible. Instead, we performed retrospective Bayesian optimization using the existing competitive DNA amplification dataset. The data was split into training and candidate

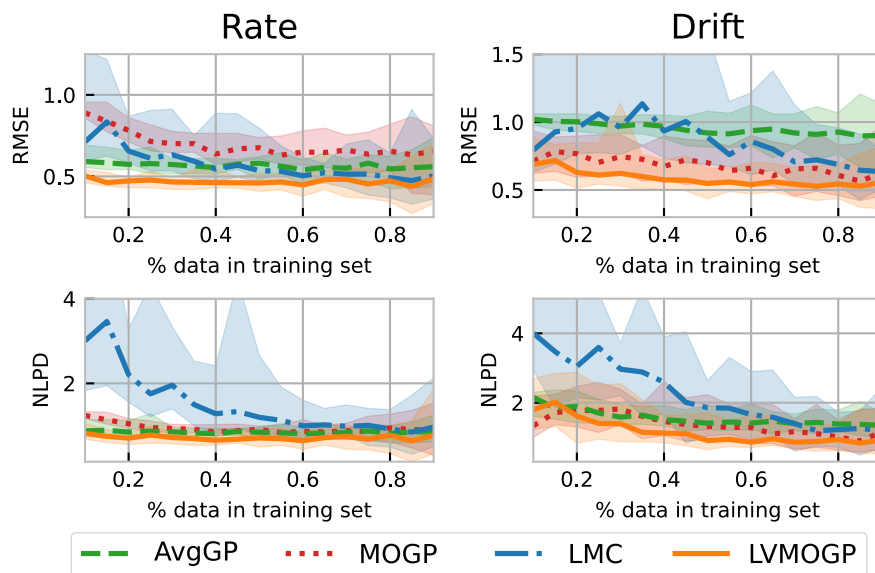


Figure 5: Results of cross-validation on the DNA amplification data for both rate and drift. For each cross-validation run, the training set consisted of all the data from two competitors and a random subset of the data on the remaining competitors, ensuring all competitors had at least one data point. This is repeated for different percentages of data in the training set, and for each percentage, it is repeated 200 times.

sets, with the design of experiments algorithm only allowed to choose the next point out of the candidate set. Bayesian optimization was run iteratively until all points had been selected or up to a maximum number of iterations, whichever happened first.

Two learning scenarios were tested: the "Learning Many" scenario where all data from two competitors were fully observed to begin with and then 16 competitors optimized in parallel; and the "One at a Time" where each of the 16 competitors was optimized individually, with the 33 remaining competitors included in the training set. These scenarios replicate likely wet lab experimentation scenarios — the first for when many competitors need to be optimized at once, and the second for when many competitors are already optimized and we want to add an extra one. The maximum number of iterations was 15 for the rate-only optimization and 20 or 10 for the penalized optimization, depending on the learning scenario.

We also considered two methods for choosing the first experiment for a new competitor with no previously observed data. Choosing the most central data point ("Center" in Figure 6) offers both maximum reduction in variance across the response surface and ensures all competitor response surfaces have a comparable point, which may help the transfer learning methods determine their similarities. It is also a reasonable approximation to what a human experimenter might do if they had no prior knowledge of the response surface. The second method is to let the Gaussian process model choose the first point ("Model's Choice" in Figure 6) for a new competitor. For the AvgGP and the LVMOGP, this is possible as they can make posterior predictions on new response surface. For the LVMOGP, the latent variable of the new surface is determined as a weighted average of the latent variables of the response surfaces with data that have the same probe and at least one matching primer. If there are no surfaces with matching primers, we use a weighted average of the surfaces with the same probe. For the LMC and MOGP we have no posterior, so the first point is selected randomly.

3.3.1 Single Objective Bayesian Optimization

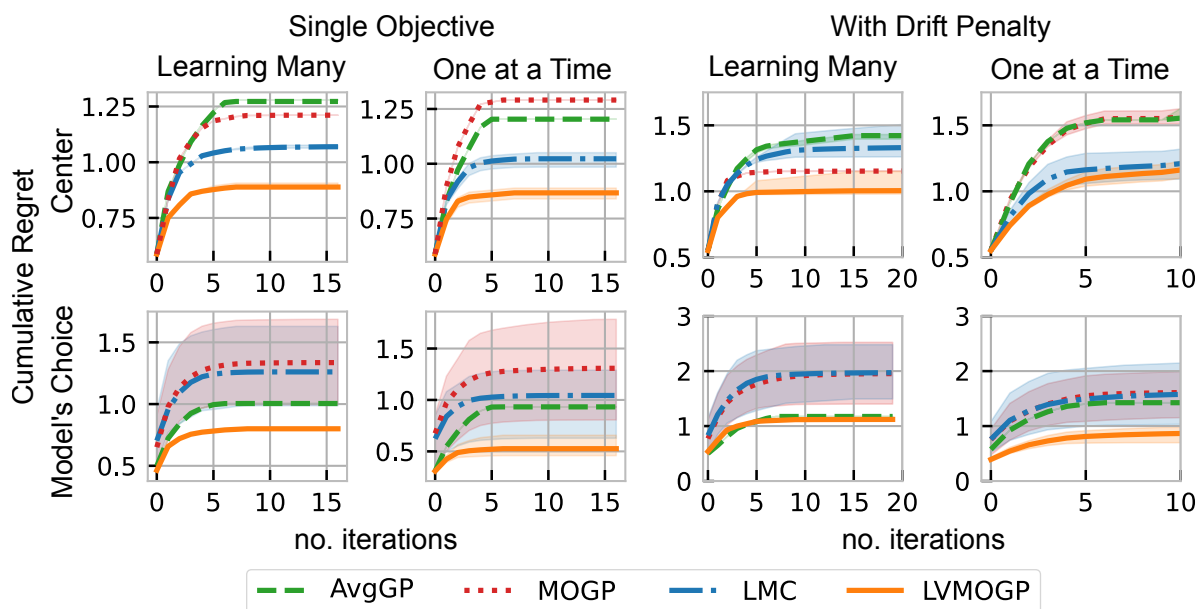


Figure 6: Cumulative regret of each of the Gaussian process models for single objective (left) and penalized (right) Bayesian optimization. Each line indicates the mean across 24 random seeds and all competitors, while the shaded regions indicate the upper and lower 5% quantiles by random seed. The top row is when the first point on each new surface is selected as being the center point, and the bottom is when the model is allowed to choose the first point. The "Learning Many" scenario is when many competitors are being optimized at the same time, and the "One at a Time" scenario is when one competitor is being optimized, with all others being in the training set.

The left panel of Figure 6 shows the results of optimizing rate without considering the drift penalty. The variance in the results comes from three sources. The first is the random selection of the next point when two points have the same expected improvement — this causes unavoidable variation. The second is due to the Gaussian process models optimizing to different hyperparameter values due to different initializations. The different values arise because the optimization of the non-convex hyperparameter loss surfaces is difficult. The final source of variation is the random starting point for the MOGP and LMC.

In all cases, the LVMOGP has much lower cumulative regret than the other models. The "Center" start point allows us to compare the performance of the Gaussian process models without being skewed by the first point. In this case the LMC and LVMOGP have the lowest cumulative regret. The ordering changes between the "Center" and "Model's choice" scenario, as in the latter the AvgGP and LVMOGP are able to predict on new surfaces, giving them an advantage over the LMC and MOGP when choosing the first point. See Appendix 8.4.3 for a table of the mean regrets of the first points for a quantification of this improvement.

As the "One at a Time" scenario includes the data from all other competitors, the Gaussian process models start with far more data than the "Learning Many" scenario. This means the AvgGP, LMC and LVMOGP all have less regret in the "One at a Time" scenario, as they are able to transfer information about the function values of competitors to improve prediction of the target competitor behavior. The MOGP does not transfer information about function values, so performs relatively worse than the others for the "One at a Time" scenario.

3.3.2 Bayesian Optimization with Drift Penalty

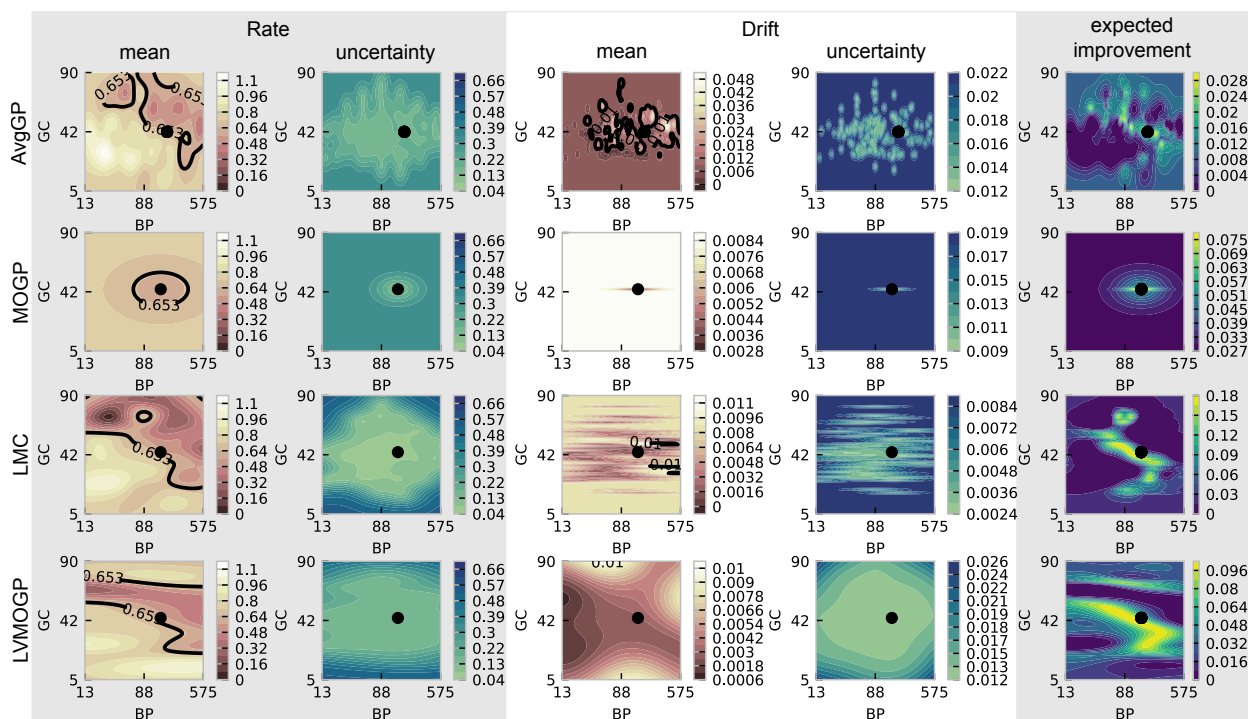


Figure 7: Predictions for the rate and drift for each of the Gaussian process models. The BP and GC axes are in log and logit scales respectively. These plots show the mean of the Gaussian process model predictions and the uncertainty which here is $2 \times$ standard deviation. The expected improvement with probability of feasibility is then plotted in the final column. This is for the case where we are optimizing competitor FP005-FP004-EvaGreen and have observed one data point so far, with the models able to choose the first point. The black contour lines on the mean plots indicate the target rate and threshold drift values.

The right-hand panel of Figure 6 shows the cumulative regret for optimization of the rate with a penalty on the drift. In all cases, the LVMOGP has the lowest cumulative regret at the end. In the "Learning Many" scenario the AvgGP again benefits from selecting the first point for the "Model's Choice" starting point, but the LVMOGP actually performs slightly worse than it did for the "Center" start point. This may be due to negative transfer in the drift predictions at very low data regimes making the selection of the first point sub-optimal.

The ordering of the Gaussian process models is different for the "Learning Many" and "One at a Time", probably because the increased amount of data allows the LMC to predict comparatively better in the "One at a Time" scenario than the "Learning Many". The LVMOGP outperforms the other Gaussian process models the most in the "One at a Time" "Model's Choice" experiment, which is likely due to the large amounts of data on all competitors, except the target, and effective transfer of information between them.

Figure 7 shows the rate and drift predictions and expected improvement for one iteration. Most notably, the MOGP has no transfer learning, so has almost equal expected improvement for most of the candidate points. The other three models transfer information across the competitors, meaning even with one data point, they have much more complex predictions than the MOGP. We can also see how the AvgGP, MOGP and LMC fit the drift poorly. This is because the drift is of a different order of

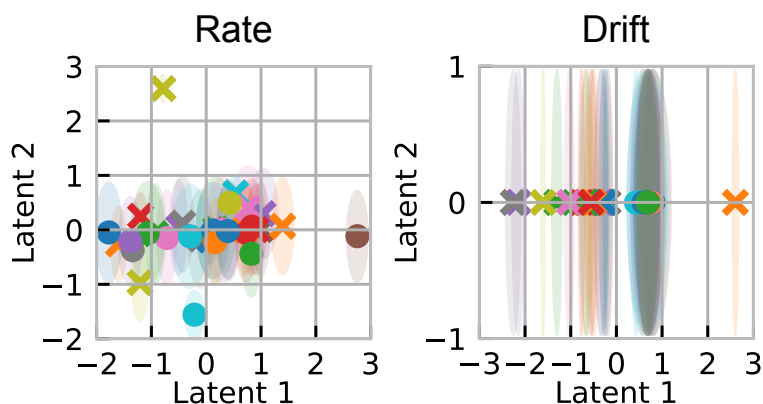


Figure 8: Latent space of the LVMOGP for the rate and drift. The crosses indicate competitors with probe primers and the dots indicate those with EvaGreen primers. The shaded circles indicate the uncertainty in the latent positions.

magnitude depending on the fluorescent probe used. Most of the Gaussian process models are unable to detect this, meaning they end up with a poor fit to the data. The LVMOGP, however, does identify this —Figure 8 shows how it clusters the two probe types at different sides of the latent space. This indicates it has recognized there are two regimes for drift, despite not being explicitly told which probe a competitor uses.

See Appendix 8.4 for further Bayesian optimization results for both the single objective and penalized optimizations. These results show the LVMOGP reaches the best point on the surfaces faster and with less cumulative regret, more often than the other models for most test cases.

4 Discussion

Expensive and time consuming experiments require an intelligent design of experiments strategy. This study demonstrates how a transfer learning surrogate model can be used in conjunction with Bayesian optimization to optimize biological sequences. For the specific case of designing competitor DNA molecules for a new diagnostic, reducing the number and therefore cost of experiments can help it reach the affordability criteria for point of care settings (Land et al., 2019).

In Bayesian optimization, we need a surrogate function with reliable mean and uncertainty estimates to ensure a balance between exploration and exploitation when selecting new points. Our cross-validation results in Section. 3.2 show the LVMOGP has better predictive accuracy than the other Gaussian process models for both rate and drift. These results also demonstrate one of the limitations of the LMC: the LMC has very high NLPD at low data regimes. This implies the LMC has poor uncertainty estimates and is overfitting, a result which has been previously observed (Dai et al., 2017).

To replicate a real-life iterative design of experiments regime, we performed Bayesian optimization on DNA amplification experimental data, but only allowing the models to select new points from existing data. For the single objective optimization case, the LVMOGP has lower cumulative regret than the other Gaussian process models for all test cases and starting points. This shows the LVMOGP transfer learning approach is useful both when optimizing multiple competitors at a time, and when using the data from all previous competitors to optimize a new one. The superior performance of the LMC and LVMOGP for the "Center" starting point shows transfer learning speeds up the learning process. These results also demonstrate the advantage of a surrogate model that can predict unseen surfaces — both the LVMOGP and the AvgGP see a large improvement in regret when they are allowed to select the first

point, both outperforming the MOGP and LMC where the first point is chosen at random.

When optimizing new biological sequences, there are often factors we wish to keep within a certain range such as purity (Degerman et al., 2006) or biophysical properties (Khan et al., 2023). While these can be treated as constraints, sometimes we may be willing to violate them slightly if it leads to a large improvement in the objective function. In these scenarios, we can add a penalty. To apply a penalty on the nuisance drift factor, we used probability of feasibility to penalize any point predicted to be above the threshold drift value. In the penalized optimization, the LVMOGP had less cumulative regret than the other models but the difference in performance was smaller than that of the single objective optimization. This could be due to the added challenge of dealing with the penalized on drift.

There was variation in the performance of the Gaussian process models' across random seeds due to the hyperparameter initialization. The LVMOGP has more variation due to its training being a harder optimization problem. While smart initialization and random restarts helped with this issue, future work could simplify the optimization procedures. The optimization of the Gaussian process models is discussed in Appendix 8.5.

While the workflow outlined here will be useful for the optimization of new competitor DNA molecules, it is not specific to this application and could be used for other applications where it is necessary to optimize many similar tasks, such as engineering DNA probes (Lopez et al., 2018; Wadle et al., 2016), exploring protein fitness landscapes (Hu et al., 2023), optimizing conditions for different cell lines (Hutter et al., 2021), or inferring psuedotime for cellular processes (Campbell and Yau, 2015). With the rise in lab automation, this workflow can be integrated into a design build test pipeline similar to Carbonell et al. (2018) and HamediRad et al. (2019) which can greatly reduce the time required to optimize new biomolecular components, speeding up the creation of new devices. This method could also be incorporated into hybrid models in bio-processing and chemical engineering, for decision making for systems with many similar components (Narayanan et al., 2023; Mowbray et al., 2021; Schweidtmann et al., 2021).

This workflow could also be extended to multi-output optimization problems by using a multi-output acquisition function or by finding Pareto optimal solutions (Belanger et al., 2019; Selega and Campbell, 2022; Jablonka et al., 2021; Schweidtmann et al., 2018). Similarly, the surrogate functions needed for multi-fidelity learning, where we have multiple sources of information about an optimization task with some sources being cheaper but less informative than others, are similar to those for transfer learning, making it an easy extension (Folch et al., 2023; Sun et al., 2022).

5 Conclusion

We have shown how a transfer learning design of experiments workflow can be used to optimize many competitor DNA molecules for an amplification-based diagnostics device. We used cross-validation to demonstrate that the latent variable multi-output Gaussian process has the best predictive accuracy and have shown it has the least regret when Bayesian optimization is performed on the DNA amplification data. Future improvements to the optimization of the model hyperparameters would lead to faster and more consistent performance of the algorithm. Despite this, we believe this workflow is applicable to many other biotechnology applications and should be used to reduce the experimental load when there are many similar tasks to be optimized but their similarity is a priori unknown.

6 Funding Information

This work was supported by the UKRI CDT in AI for Healthcare Grant No. EP/S023283/1, UK Research and Innovation Grant No. EP/P016871/1, the BASF / RAEng Research Chair in Data-Driven

Optimization, the US NIH Grant No. 5F32GM131594, the EPSRC IRC Next Steps Plus grant No. EP/R018707/1 and the RAEng Chair in Emerging Technologies award No. CiET2021/ 94. For the purpose of open access, the authors have applied a Creative Commons Attribution (CC BY) licence to any Author Accepted Manuscript version arising.

7 Conflict of Interest

JPG and MMS are co-founders at Signatur Biosciences, Inc., a company which seeks to commercialize the medical diagnostic technology this paper focuses on as a use-case, and they are co-inventors in a patent describing a method for amplification-based quantification of nucleic acids. The remaining authors declare no conflict of interest.

References

- Badeau, B. A., Comerford, M. P., Arakawa, C. K., Shadish, J. A. and DeForest, C. A. (2018) Engineered modular biomaterial logic gates for environmentally triggered therapeutic delivery. *Nature chemistry*, **10**, 251–258. URL: <https://www.ncbi.nlm.nih.gov/pmc/articles/PMC5822735/>.
- Bader, J., Narayanan, H., Arosio, P. and Leroux, J.-C. (2023) Improving extracellular vesicles production through a Bayesian optimization-based experimental design. *European Journal of Pharmaceutics and Biopharmaceutics*, **182**, 103–114. URL: <https://www.sciencedirect.com/science/article/pii/S0939641122002983>.
- Belanger, D., Vora, S., Mariet, Z., Deshpande, R., Dohan, D., Angermueller, C., Murphy, K., Chapelle, O. and Colwell, L. (2019) Biological Sequences Design using Batched Bayesian Optimization.
- Blakney, A. K., McKay, P. F., Ibarzo Yus, B., Hunter, J. E., Dex, E. A. and Shattock, R. J. (2019) The Skin You Are In: Design-of-Experiments Optimization of Lipid Nanoparticle Self-Amplifying RNA Formulations in Human Skin Explants. *ACS Nano*, **13**, 5920–5930. URL: <https://pubs.acs.org/doi/10.1021/acsnano.9b01774>.
- Bonilla, E. V., Chai, K. and Williams, C. (2007) Multi-task Gaussian Process Prediction. *Advances in Neural Information Processing Systems*, **20**. URL: <https://proceedings.neurips.cc/paper/2007/hash/66368270ffd51418ec58bd793f2d9b1b-Abstract.html>.
- Campbell, K. and Yau, C. (2015) Bayesian Gaussian Process Latent Variable Models for pseudotime inference in single-cell RNA-seq data.
- Cao, B., Pan, S. J., Zhang, Y., Yeung, D.-Y. and Yang, Q. (2010) Adaptive Transfer Learning. *Proceedings of the AAAI Conference on Artificial Intelligence*, **24**. URL: <https://ojs.aaai.org/index.php/AAAI/article/view/7682>. Number: 1.
- Carbonell, P., Jervis, A. J., Robinson, C. J., Yan, C., Dunstan, M., Swainston, N., Vinaixa, M., Hollywood, K. A., Currin, A., Rattray, N. J. W., Taylor, S., Spiess, R., Sung, R., Williams, A. R., Fellows, D., Stanford, N. J., Mulherin, P., Le Feuvre, R., Barran, P., Goodacre, R., Turner, N. J., Goble, C., Chen, G. G., Kell, D. B., Micklefield, J., Breitling, R., Takano, E., Faulon, J.-L. and Scrutton, N. S. (2018) An automated Design-Build-Test-Learn pipeline for enhanced microbial production of fine chemicals. *Communications Biology*, **1**, 1–10. URL: <https://www.nature.com/articles/s42003-018-0076-9>. Number: 1 Publisher: Nature Publishing Group.
- Cox, D. R. and Reid, N. (2000) *The Theory of the Design of Experiments*. CRC Press.
- Dai, Z., Álvarez, M. and Lawrence, N. (2017) Efficient Modeling of Latent Information in Supervised Learning using Gaussian Processes. In *Advances in Neural Information Processing Systems*, vol. 30. Curran Associates, Inc. URL: <https://proceedings.neurips.cc/paper/2017/file/1680e9fa7b4dd5d62ece800239bb53bd-Paper.pdf>.
- Degerman, M., Jakobsson, N. and Nilsson, B. (2006) Constrained optimization of a preparative ion-exchange step for antibody purification. *Journal of Chromatography A*, **1113**, 92–100. URL: <https://www.sciencedirect.com/science/article/pii/S0021967306003013>.
- Deng, F., Pan, J., Liu, Z., Zeng, L. and Chen, J. (2023) Programmable DNA biocomputing circuits for rapid and intelligent screening of SARS-CoV-2 variants. *Biosensors and Bioelectronics*, **223**, 115025. URL: <https://www.sciencedirect.com/science/article/pii/S095656632201065X>.

- Droettboom, M., Hunter, J., Firing, E., Caswell, T. A., Elson, P., Dale, D., Lee, J.-J., McDougall, D., Root, B., Straw, A., Seppänen, J. K., Nielsen, J. H., May, R., Varoquaux, Yu, T. S., Moad, C., Gohlke, C., Würtz, P., Hisch, T., Silvester, S., Ivanov, P., Whitaker, J., Cimarron, Hobson, P., Giuca, M., Thomas, I., mmetz bn, Evans, J., dhyams and NNemec (2015) matplotlib: v1.4.3. URL: <https://zenodo.org/record/15423>.
- Ebrahimi, S. B. and Samanta, D. (2023) Engineering protein-based therapeutics through structural and chemical design. *Nature Communications*, **14**, 2411. URL: <https://www.nature.com/articles/s41467-023-38039-x>. Number: 1 Publisher: Nature Publishing Group.
- Fellermann, H., Shirt-Ediss, B., Kozyra, J., Linsley, M., Lendrem, D., Isaacs, J. and Howard, T. (2019) Design of experiments and the virtual PCR simulator: An online game for pharmaceutical scientists and biotechnologists. *Pharmaceutical Statistics*, **18**, 402–406. URL: <https://www.ncbi.nlm.nih.gov/pmc/articles/PMC6767770/>.
- Folch, J. P., Lee, R. M., Shafei, B., Walz, D., Tsay, C., van der Wilk, M. and Misener, R. (2023) Combining multi-fidelity modelling and asynchronous batch Bayesian Optimization. *Computers & Chemical Engineering*, **172**, 108194. Publisher: Elsevier.
- Gamble, C., Bryant, D., Carrieri, D., Bixby, E., Dang, J., Marshall, J., Doughty, D., Colwell, L., Berndl, M., Roberts, J. and Frumkin, M. (2021) Machine Learning Optimization of Photosynthetic Microbe Cultivation and Recombinant Protein Production. *preprint*, Bioengineering. URL: <http://biorxiv.org/lookup/doi/10.1101/2021.08.06.453272>.
- Garnett, R. (2023) Bayesian Optimization. 127–129. Cambridge University Press.
- Gilman, J., Walls, L., Bandiera, L. and Menolascina, F. (2021) Statistical Design of Experiments for Synthetic Biology. *ACS Synthetic Biology*, **10**, 1–18. URL: <https://doi.org/10.1021/acssynbio.0c00385>. Publisher: American Chemical Society.
- Goertz, J. P., Sedgwick, R., Smith, F., Kaforou, M., Wright, V. J., Herberg, J. A., Kote-Jarai, Z., Eeles, R., Levin, M., Misener, R., Wilk, M. v. d. and Stevens, M. M. (2023) Competitive Amplification Networks enable molecular pattern recognition with PCR. URL: <https://www.biorxiv.org/content/10.1101/2023.06.29.546934v1>.
- González, J., Longworth, J., James, D. C. and Lawrence, N. D. (2015) Bayesian Optimization for Synthetic Gene Design. *arXiv:1505.01627 [stat]*. URL: <http://arxiv.org/abs/1505.01627>. ArXiv: 1505.01627.
- HamediRad, M., Chao, R., Weisberg, S., Lian, J., Sinha, S. and Zhao, H. (2019) Towards a fully automated algorithm driven platform for biosystems design. *Nature Communications*, **10**, 5150. URL: <https://www.nature.com/articles/s41467-019-13189-z>. Number: 1 Publisher: Nature Publishing Group.
- Harris, C. R., Millman, K. J., van der Walt, S. J., Gommers, R., Virtanen, P., Cournapeau, D., Wieser, E., Taylor, J., Berg, S., Smith, N. J., Kern, R., Picus, M., Hoyer, S., van Kerkwijk, M. H., Brett, M., Haldane, A., del Río, J. F., Wiebe, M., Peterson, P., Gérard-Marchant, P., Sheppard, K., Reddy, T., Weckesser, W., Abbasi, H., Gohlke, C. and Oliphant, T. E. (2020) Array programming with NumPy. *Nature*, **585**, 357–362. URL: <https://www.nature.com/articles/s41586-020-2649-2>. Number: 7825 Publisher: Nature Publishing Group.

- Hie, B., Bryson, B. D. and Berger, B. (2020) Leveraging Uncertainty in Machine Learning Accelerates Biological Discovery and Design. *Cell Systems*, **11**, 461–477.e9. URL: [https://www.cell.com/cell-systems/abstract/S2405-4712\(20\)30364-1](https://www.cell.com/cell-systems/abstract/S2405-4712(20)30364-1). Publisher: Elsevier.
- Hu, R., Fu, L., Chen, Y., Chen, J., Qiao, Y. and Si, T. (2023) Protein engineering via Bayesian optimization-guided evolutionary algorithm and robotic experiments. *Briefings in Bioinformatics*, **24**, bbac570. URL: <https://doi.org/10.1093/bib/bbac570>.
- Hua, Y., Ma, J., Li, D. and Wang, R. (2022) DNA-Based Biosensors for the Biochemical Analysis: A Review. *Biosensors*, **12**, 183. URL: <https://www.ncbi.nlm.nih.gov/pmc/articles/PMC8945906/>.
- Hutter, C., von Stosch, M., Cruz Bournazou, M. N. and Butté, A. (2021) Knowledge transfer across cell lines using hybrid Gaussian process models with entity embedding vectors. *Biotechnology and Bioengineering*, **118**, 4389–4401. URL: <https://onlinelibrary.wiley.com/doi/abs/10.1002/bit.27907>.
- Jablonka, K. M., Jothiappan, G. M., Wang, S., Smit, B. and Yoo, B. (2021) Bias free multiobjective active learning for materials design and discovery. *Nature Communications*, **12**, 2312. URL: <https://www.nature.com/articles/s41467-021-22437-0>. Number: 1 Publisher: Nature Publishing Group.
- Jones, D. R., Schonlau, M. and Welch, W. J. (1998) Efficient Global Optimization of Expensive Black-Box Functions. *Journal of Global Optimization*, **13**, 455–492. URL: <https://doi.org/10.1023/A:1008306431147>.
- Khan, A., Cowen-Rivers, A. I., Grosnit, A., Deik, D.-G.-X., Robert, P. A., Greiff, V., Smorodina, E., Rawat, P., Akbar, R., Dreckowski, K., Tutunov, R., Bou-Ammar, D., Wang, J., Storkey, A. and Bou-Ammar, H. (2023) Toward real-world automated antibody design with combinatorial Bayesian optimization. *Cell Reports Methods*, **3**, 100374.
- Kreutz, C. and Timmer, J. (2009) Systems biology: experimental design. *The FEBS journal*, **276**, 923–942.
- Land, K. J., Boeras, D. I., Chen, X.-S., Ramsay, A. R. and Peeling, R. W. (2019) REASSURED diagnostics to inform disease control strategies, strengthen health systems and improve patient outcomes. *Nature Microbiology*, **4**, 46–54. URL: <https://www.nature.com/articles/s41564-018-0295-3>. Number: 1 Publisher: Nature Publishing Group.
- Lopez, R., Wang, R. and Seelig, G. (2018) A molecular multi-gene classifier for disease diagnostics. *Nature Chemistry*, **10**, 746–754. URL: <https://www.nature.com/articles/s41557-018-0056-1>. Number: 7 Publisher: Nature Publishing Group.
- Lv, H., Li, Q., Shi, J., Fan, C. and Wang, F. (2021) Biocomputing Based on DNA Strand Displacement Reactions. *ChemPhysChem*, **22**, 1151–1166. URL: <https://onlinelibrary.wiley.com/doi/abs/10.1002/cphc.202100140>.
- Lyu, W., Xue, P., Yang, F., Yan, C., Hong, Z., Zeng, X. and Zhou, D. (2018) An Efficient Bayesian Optimization Approach for Automated Optimization of Analog Circuits. *IEEE Transactions on Circuits and Systems I: Regular Papers*, **65**, 1954–1967. Conference Name: IEEE Transactions on Circuits and Systems I: Regular Papers.

- Matthews, A. G., Van Der Wilk, M., Nickson, T., Fujii, K., Boukouvalas, A., León-Villagrà, P., Ghahramani, Z. and Hensman, J. (2017) GPflow: a Gaussian process library using tensorflow. *The Journal of Machine Learning Research*, **18**, 1299–1304.
- Mehrian, M., Guyot, Y., Papantoniou, I., Olofsson, S., Sonnaert, M., Misener, R. and Geris, L. (2018) Maximizing neotissue growth kinetics in a perfusion bioreactor: An in silico strategy using model reduction and Bayesian optimization. *Biotechnology and Bioengineering*, **115**, 617–629. URL: <https://onlinelibrary.wiley.com/doi/abs/10.1002/bit.26500>.
- Mowbray, M., Savage, T., Wu, C., Song, Z., Cho, B. A., Del Rio-Chanona, E. A. and Zhang, D. (2021) Machine learning for biochemical engineering: A review. *Biochemical Engineering Journal*, **172**, 108054. URL: <https://www.sciencedirect.com/science/article/pii/S1369703X21001303>.
- Narayanan, H., Dingfelder, F., Condado Morales, I., Patel, B., Heding, K. E., Bjelke, J. R., Egebjerg, T., Butté, A., Sokolov, M., Lorenzen, N. and Arosio, P. (2021) Design of Biopharmaceutical Formulations Accelerated by Machine Learning. *Molecular Pharmaceutics*, **18**, 3843–3853. URL: <https://pubs.acs.org/doi/10.1021/acs.molpharmaceut.1c00469>.
- Narayanan, H., Luna, M. F., von Stosch, M., Cruz Bournazou, M. N., Polotti, G., Morbidelli, M., Butté, A. and Sokolov, M. (2020) Bioprocessing in the Digital Age: The Role of Process Models. *Biotechnology Journal*, **15**, 1900172. URL: <https://onlinelibrary.wiley.com/doi/abs/10.1002/biot.201900172>.
- Narayanan, H., von Stosch, M., Feidl, F., Sokolov, M., Morbidelli, M. and Butté, A. (2023) Hybrid modeling for biopharmaceutical processes: advantages, opportunities, and implementation. *Frontiers in Chemical Engineering*, **5**. URL: <https://www.frontiersin.org/articles/10.3389/fceng.2023.1157889>.
- Papaneophytou, C. (2019) Design of Experiments As a Tool for Optimization in Recombinant Protein Biotechnology: From Constructs to Crystals. *Molecular Biotechnology*, **61**, 873–891. URL: <https://doi.org/10.1007/s12033-019-00218-x>.
- Politis, S. N., Colombo, P., Colombo, G. and Rekkas, D. M. (2017) Design of experiments (DoE) in pharmaceutical development. *Drug Development and Industrial Pharmacy*, **43**, 889–901. URL: <https://doi.org/10.1080/03639045.2017.1291672>.
- Qian, L., Winfree, E. and Bruck, J. (2011) Neural network computation with DNA strand displacement cascades. *Nature*, **475**, 368–372. URL: <https://www.nature.com/articles/nature10262>.
- Rasmussen, C. E. and Williams, C. K. I. (2006) *Gaussian processes for machine learning*. Adaptive computation and machine learning. Cambridge, Mass: MIT Press.
- Romero, P. A., Krause, A. and Arnold, F. H. (2013) Navigating the protein fitness landscape with Gaussian processes. *Proceedings of the National Academy of Sciences*, **110**, E193–E201. URL: <https://www.pnas.org/content/110/3/E193>. Publisher: National Academy of Sciences Section: PNAS Plus.
- Rosa, S. S., Nunes, D., Antunes, L., Prazeres, D. M. F., Marques, M. P. C. and Azevedo, A. M. (2022) Maximizing mRNA vaccine production with Bayesian optimization. *Biotechnology and Bioengineering*, **119**, 3127–3139. URL: <https://onlinelibrary.wiley.com/doi/abs/10.1002/bit.28216>.

- Salvatier, J., Wiecki, T. V. and Fonnesbeck, C. (2016) Probabilistic programming in Python using PyMC3. *PeerJ Computer Science*, **2**, e55. URL: <https://peerj.com/articles/cs-55>. Publisher: PeerJ Inc.
- Schonlau, M., Welch, W. J. and Jones, D. R. (1998) Global versus local search in constrained optimization of computer models. In *New developments and applications in experimental design*, vol. 34, 11–26. Institute of Mathematical Statistics. URL: <https://projecteuclid.org/ebooks/institute-of-mathematical-statistics-lecture-notes-monograph-series/New-developments-and-applications-in-experimental-design/chapter/Global-versus-local-search-in-constrained-optimization-of-computer-models/10.1214/lnms/1215456182>.
- Schweidtmann, A. M., Clayton, A. D., Holmes, N., Bradford, E., Bourne, R. A. and Lapkin, A. A. (2018) Machine learning meets continuous flow chemistry: Automated optimization towards the Pareto front of multiple objectives. *Chemical Engineering Journal*, **352**, 277–282. URL: <https://www.sciencedirect.com/science/article/pii/S1385894718312634>.
- Schweidtmann, A. M., Esche, E., Fischer, A., Kloft, M., Repke, J.-U., Sager, S. and Mitsos, A. (2021) Machine Learning in Chemical Engineering: A Perspective. *Chemie Ingenieur Technik*, **93**, 2029–2039. URL: <https://onlinelibrary.wiley.com/doi/abs/10.1002/cite.202100083>.
- Sedgwick, R., Goertz, J., Stevens, M., Misener, R. and van der Wilk, M. (2020) Design of Experiments for Verifying Biomolecular Networks. *arXiv:2011.10575 [cs, q-bio, stat]*. URL: <http://arxiv.org/abs/2011.10575>. ArXiv: 2011.10575.
- Selega, A. and Campbell, K. R. (2022) Multi-objective Bayesian Optimization with Heuristic Objectives for Biomedical and Molecular Data Analysis Workflows. *Transactions on Machine Learning Research*. URL: <https://openreview.net/forum?id=QspAcsAyis>.
- Shahriari, B., Swersky, K., Wang, Z., Adams, R. P. and de Freitas, N. (2016) Taking the Human Out of the Loop: A Review of Bayesian Optimization. *Proceedings of the IEEE*, **104**, 148–175.
- Sharpe, C., Seepersad, C. C., Watts, S. and Tortorelli, D. (2018) Design of Mechanical Metamaterials via Constrained Bayesian Optimization. In *Volume 2A: 44th Design Automation Conference*, V02AT03A029. Quebec City, Quebec, Canada: American Society of Mechanical Engineers. URL: <https://asmedigitalcollection.asme.org/IDETC-CIE/proceedings/IDETC-CIE2018/51753/Quebec%20City,%20Quebec,%20Canada/273625>.
- Siuti, P., Yazbek, J. and Lu, T. K. (2013) Synthetic circuits integrating logic and memory in living cells. *Nature Biotechnology*, **31**, 448–452. URL: <https://www.nature.com/articles/nbt.2510>.
- Snoek, J., Larochelle, H. and Adams, R. P. (2012) Practical Bayesian Optimization of Machine Learning Algorithms. In *Advances in Neural Information Processing Systems*, vol. 25. Curran Associates, Inc. URL: <https://proceedings.neurips.cc/paper/2012/hash/05311655a15b75fab86956663e1819cd-Abstract.html>.
- Sun, Y., Nathan-Roberts, W., Pham, T. D., Otte, E. and Aickelin, U. (2022) Multi-fidelity Gaussian Process for Biomanufacturing Process Modeling with Small Data. URL: <http://arxiv.org/abs/2211.14493>. ArXiv:2211.14493 [cs].
- Swersky, K., Snoek, J. and Adams, R. P. (2013) Multi-Task Bayesian Optimization. In *Advances in Neural Information Processing Systems 26* (eds. C. J. C. Burges, L. Bottou, M. Welling, Z. Ghahramani and K. Q. Weinberger), 2004–2012. URL: <http://papers.nips.cc/paper/5086-multi-task-bayesian-optimization.pdf>.

- Taylor, C. J., Felton, K. C., Wigh, D., Jeraal, M. I., Grainger, R., Chessari, G., Johnson, C. N. and Lapkin, A. A. (2023) Accelerated Chemical Reaction Optimization Using Multi-Task Learning. *ACS Central Science*, **9**, 957–968. URL: <https://pubs.acs.org/doi/10.1021/acscentsci.3c00050>.
- The pandas development team, T. p. d. (2023) pandas-dev/pandas: Pandas. URL: <https://zenodo.org/record/7979740>.
- Tighineanu, P., Skubch, K., Baireuther, P., Reiss, A., Berkenkamp, F. and Vinogradska, J. (2022) Transfer Learning with Gaussian Processes for Bayesian Optimization. In *Proceedings of The 25th International Conference on Artificial Intelligence and Statistics*, 6152–6181. PMLR. URL: <https://proceedings.mlr.press/v151/tighineanu22a.html>. ISSN: 2640-3498.
- Titsias, M. (2009) Variational Learning of Inducing Variables in Sparse Gaussian Processes. In *Proceedings of the Twelfth International Conference on Artificial Intelligence and Statistics*, 567–574. PMLR. URL: <https://proceedings.mlr.press/v5/titsias09a.html>. ISSN: 1938-7228.
- Titsias, M. and Lawrence, N. D. (2010) Bayesian Gaussian Process Latent Variable Model. In *Proceedings of the Thirteenth International Conference on Artificial Intelligence and Statistics*, 844–851. JMLR Workshop and Conference Proceedings. URL: <https://proceedings.mlr.press/v9/titsias10a.html>. ISSN: 1938-7228.
- Uhrenholt, A. K. and Jensen, B. S. (2019) Efficient Bayesian Optimization for Target Vector Estimation. In *Proceedings of the Twenty-Second International Conference on Artificial Intelligence and Statistics* (eds. K. Chaudhuri and M. Sugiyama), vol. 89 of *Proceedings of Machine Learning Research*, 2661–2670. PMLR. URL: <https://proceedings.mlr.press/v89/uhrenholt19a.html>.
- Virtanen, P., Gommers, R., Oliphant, T. E., Haberland, M., Reddy, T., Cournapeau, D., Burovski, E., Peterson, P., Weckesser, W., Bright, J., van der Walt, S. J., Brett, M., Wilson, J., Millman, K. J., Mayorov, N., Nelson, A. R. J., Jones, E., Kern, R., Larson, E., Carey, C. J., Polat, I., Feng, Y., Moore, E. W., VanderPlas, J., Laxalde, D., Perktold, J., Cimrman, R., Henriksen, I., Quintero, E. A., Harris, C. R., Archibald, A. M., Ribeiro, A. H., Pedregosa, F. and van Mulbregt, P. (2020) SciPy 1.0: fundamental algorithms for scientific computing in Python. *Nature Methods*, **17**, 261–272. URL: <https://www.nature.com/articles/s41592-019-0686-2>. Number: 3 Publisher: Nature Publishing Group.
- Wadle, S., Lehnert, M., Rubenwolf, S., Zengerle, R. and von Stetten, F. (2016) Real-time PCR probe optimization using design of experiments approach. *Biomolecular Detection and Quantification*, **7**, 1–8. URL: <https://www.sciencedirect.com/science/article/pii/S2214753515300139>.
- Zadeh, J. N., Steenberg, C. D., Bois, J. S., Wolfe, B. R., Pierce, M. B., Khan, A. R., Dirks, R. M. and Pierce, N. A. (2011) NUPACK: Analysis and design of nucleic acid systems. *Journal of Computational Chemistry*, **32**, 170–173. URL: <https://onlinelibrary.wiley.com/doi/abs/10.1002/jcc.21596>.
- Zhang, Y., Tao, S., Chen, W. and Apley, D. W. (2020) A Latent Variable Approach to Gaussian Process Modeling with Qualitative and Quantitative Factors. *Technometrics*, **62**, 291–302. URL: <https://www.tandfonline.com/doi/full/10.1080/00401706.2019.1638834>.
- Zhuang, F., Qi, Z., Duan, K., Xi, D., Zhu, Y., Zhu, H., Xiong, H. and He, Q. (2021) A Comprehensive Survey on Transfer Learning. *Proceedings of the IEEE*, **109**, 43–76. Conference Name: Proceedings of the IEEE.

Álvarez, M. A., Rosasco, L. and Lawrence, N. D. (2012) Kernels for Vector-Valued Functions: A Review. *Foundations and Trends® in Machine Learning*, 4, 195–266. URL: <https://www.nowpublishers.com/article/Details/MAL-036>. Publisher: Now Publishers, Inc.

8 Appendix

Nomenclature

Acronyms

AvgGP Average Gaussian Process

BP Number of Base Pairs

DNA Deoxyribonucleic Acid

ELBO Evidence lower bound to marginal likelihood for LVMOGP

GC Percentage Guanine-Cytosine Content

LMC Linear Model of Coregionalization

LVMOGP Latent Variable Multi-output Gaussian Process

MOGP Multi-output Gaussian Process

NLPD Negative Log Predictive Density

PCR Polymerase Chain Reaction

RMSE Root Mean Squared Error

Functions

$\alpha_{EI}(\cdot)$ Expected improvement acquisition function

$\alpha_p(\cdot)$ Acquisition function including probability of feasibility

\mathcal{GP} Gaussian Process

$f(\cdot)$ Function of \mathbf{x}

$f_{\text{rate}}(\cdot)$ Rate function in competitor amplification

$f_{\text{drift}}(\cdot)$ Drift function

$g(\cdot)$ Latent Gaussian processes in the linear model of coregionalisation

$k(\cdot, \cdot)$ Gaussian Process covariance function

$K_{ij}(\cdot, \cdot)$ Covariance function of the data

$K_{iu}(\cdot, \cdot)$ Cross covariance function between the data and inducing points

$K_{uu}(\cdot, \cdot)$ Covariance function of the inducing points

$m(\cdot)$ Gaussian Process mean function

$PF(\cdot)$ Probability of feasibility

Parameters and Variables

δ	stochastic variable defined as the squared difference between observed outputs and the target value
\mathbf{f}_*	Predictions at locations X_*
\mathbf{h}_p	Latent variable of the p^{th} output function
\mathbf{I}	Identity matrix
\mathbf{u}	Inducing variables
\mathbf{W}	Vector of weights of the latent functions in the linear model of coregionalisation
\mathbf{x}	Input location such that $\mathbf{x} \in \mathbb{R}^D$
ℓ_d	Lengthscale of dimension d
ϵ	Noise added to y where $\epsilon \sim \mathcal{N}(0, \sigma_n^2 \mathbf{I})$
λ	Non-centrality parameter of target vector optimization expected improvement
$\mu(X_*)$	Predicted mean at locations X_*
μ_{h_p}	Mean of the p^{th} latent variable
ν	Carrying capacity
$\sigma(X_*)$	Predicted covariance at locations X_*
σ_k^2	Kernel variance
σ_n^2	Noise variance of Gaussian process
Σ_{h_p}	Variance of the p^{th} latent variable
τ	Cycle number
θ	Gaussian Process hyperparameters
B	Coregionalization matrix in the LMC
D	Dimensions of \mathbf{x}
F	Fluorescence in DNA amplification reaction
F_0	Fluorescence at the beginning of the DNA amplification reaction
F_T	Fluorescence at the end of the DNA amplification reaction
H	Latent variables such that $H = [\mathbf{h}_1, \dots, \mathbf{h}_p]^T \in \mathbb{R}^{Q_H \times P}$
M	Mean of the variational distribution on Z
P	Number of output functions in multi-output Gaussian Process
$q(\cdot)$	Variational distribution
Q	Number of covariance matrices in the LMC

- S Variance of the variational distribution on Z
- $t = \delta\gamma^{-2}$
- T_{rate} Target rate
- T_{drift} Drift threshold
- X Training inputs of Gaussian Process $X = \{\mathbf{x}_1, \dots, \mathbf{x}_N\} \in \mathbb{R}^{N \times D}$
- X_* Locations to be evaluated
- y Noisy evaluations of \mathbf{x}
- y_{best} Data point which is closest to the target out of the train and test datasets for a given surface
- Z Inducing points

Miscellaneous

- \mathcal{H} The latent space in the LVMOGP
- G An approximation to the cumulative non-central χ^2 distribution function

8.1 Latent Variable Multi-output Gaussian Process Implementation

Gaussian processes are normally trained by maximizing the log marginal likelihood. However, the presence of the latent variable distributions in the LVMOGP means the log marginal likelihood is no longer tractable. Instead, Dai et al. (2017) used variational inference to approximate a lower bound to this log marginal likelihood, following the method proposed by Titsias (2009) and Titsias and Lawrence (2010). In variational inference, the aim is to minimize the Kullback-Leibler divergence between an approximate posterior and a true posterior.

Our implementation of the LVMOGP takes a concatenation of the input data and their corresponding latent variables $\tilde{X} = [X, H:] \in \mathbb{R}^{N \times (D+Q_H)}$ where H_i denotes the vector of latent inputs for each observed data point. All inputs X_p for the same output dimension will have the same latent variable, h_p .

For the LVMOGP this variational lower bound is given as:

$$\begin{aligned}
 ELBO = & -\frac{1}{2} \log(2\pi\sigma_n^2) + \sum_{i=1}^N \left[-\frac{1}{2\sigma_n^2} y_{:i}^T y_{:i} + \frac{1}{\sigma_n^2} y_{:i} \langle K_{iu} \rangle_{q(H_i)} K_{uu}^{-1} M \right. \\
 & - \frac{1}{2\sigma_n^2} \text{Tr}(K_{uu}^{-1} \langle K_{iu}^T K_{iu} \rangle_{q(H_i)} K_{uu}^{-1} (MM^T + S)) \\
 & \left. - \frac{1}{2\sigma_n^2} (\text{Tr}(\langle K_{ii} \rangle_{q(H_i)}) - \text{Tr}(K_{uu}^{-1} \langle K_{iu}^T K_{iu} \rangle_{q(H_i)})) \right] \\
 & - KL[q(\mathbf{u})||p(\mathbf{u})] - \sum_{i=1}^N KL[q(H_i)||p(H_i)] \quad (19)
 \end{aligned}$$

where $\langle K \rangle_{q(h_i)}$ denotes a kernel expectation over the variational distribution of the latent variable of data point i . K_{ii} and K_{uu} are the covariance functions of the data and the inducing points Z respectively, while K_{iu} is the cross covariance function between the two. Tr is the trace of a matrix. M and S are the mean and covariance of the variational distribution over inducing points $q(Z) \sim \mathcal{N}(M, S)$. The second term in this expression can be viewed as a data fit term, while the last term can be seen as a complexity penalty.

Two types of prediction are relevant using the LVMOGP. The first is when we have new input points X_* and new position on the latent space h_* . In this case, the posterior prediction can be calculated in closed form. The second, and more likely, prediction case is when we want to predict a new point X_* at a point on the latent space where we already have data with latent variable h_p . This integration is intractable, but following Titsias and Lawrence (2010), the first and second moments can be computed in closed form if using a squared exponential kernel.

8.2 Data Availability

Raw data is available on request from rdm-enquiries@imperial.ac.uk. Code for the synthetic experiments can be found at the following link: <https://github.com/RSedgwick/TLGPs> Code for the DNA amplification experiments Bayesian optimization can be found here: https://github.com/RSedgwick/TL_DOE_4_DNA.

8.3 Data Summary

Each competitor is defined by its primer-reporter combination. For each of these primer-pair combinations we then have data at different guanine-cytosine content and no. of base pairs combinations. Table 1 gives a summary of the number of unique locations on each of the competitors.

Not To Be Optimized		To Be Optimized	
Primer Reporter Combination	No. Unique Locations	Primer Reporter Combination	No. Unique Locations
FP004-RP004-EvaGreen	28	FP004-RP004-Probe	53
FP002-RP002x-Probe	12	FP001-RP001x-EvaGreen	24
FP004-RP004x-Probe	12	FP001-RP001x-Probe	20
FP001-RP001-Probe	9	RP001x-FP002-Probe	19
FP001-RP005-Probe	8	FP002-RP002x-EvaGreen	15
FP004-RP004x-EvaGreen	8	FP005-FP001-EvaGreen	14
FP003-RP008-Probe	5	FP004-FP005-Probe	8
FP006-RP006-Probe	5	FP005-FP001-Probe	8
FP005-RP005-Probe	5	FP005-FP004-EvaGreen	8
FP002-RP002-EvaGreen	4	RP002x-FP005-Probe	8
FP002-RP006-Probe	4	RP008x-FP001-EvaGreen	8
FP057.1.0-RP003x-Probe	3	RP008x-FP005-Probe	8
FP003-RP008x-EvaGreen	3	FP001-RP004-EvaGreen	7
FP003-RP008-EvaGreen	3	RP002x-FP004-EvaGreen	6
FP002-RP002-Probe	3	FP002-RP004-EvaGreen	3
FP001-RP001-EvaGreen	2	RP002x-FP002-EvaGreen	2
FP003-RP003-Probe	1		
FP057.1.0-RP003x-EvaGreen	1		

Table 1: Summary of the amount of data we have for each competitor design surface. Each unique location refers to a unique GC-BP combination.

8.4 Extra Bayesian Optimization Results

The following tables contain extra results for the Bayesian optimization experiments. The first table in each section, Tables 2 and 5, shows counts of the first model to get to the best point on a surface for all competitors and seeds. If two models get to the best point on the same iteration, they are both counted as "winners". The second table, Tables 3 and 6 shows counts of the models with the lowest cumulative regret for each competitor and seed. The same thing applies if two models have the same cumulative regret. For the single objective optimization, Table 4 shows the average number of iterations for each model to get within tolerance of the target rate (± 0.05). For the penalized optimization Table 7 shows the average number of iterations for each model to get either within tolerance of the rate target with no drift penalty, or to the best point (which may have a drift penalty). For some of the runs with the drift penalty, some of the models failed to get to the best point for some surfaces within the experimental budget. In these cases, those surfaces were discarded and the average was taken for the surfaces where all the models had managed to get to the best point within the experimental budget.

8.4.1 Single Objective Optimization

Extra results for the single objective Bayesian optimization. These results demonstrate that the LVMOGP gets to the best point more often (Table 2) and has the lowest cumulative regret (Table 3) more often than the other models. The LVMOGP also reaches the best point in the lowest number of iterations for all the learning scenarios (Table 4).

learning scenario	starting point	MOGP	Avg GP	LMC	LVMOGP
learning many	center	124	121	144	255
	model's choice	107	119	97	147
one at a time	center	140	140	156	215
	model's choice	86	118	87	191

Table 2: Table showing counts of the first Gaussian process model to reach the best point on a surface for the single objective Bayesian optimization experiments. The counts are the number of times a Gaussian process model did the best on a competitor for each seed. If two Gaussian process models performed the same for a given instance, they are both counted. This is for 16 competitors and 25 random seeds.

learning scenario	starting point	MOGP	Avg GP	LMC	LVMOGP
learning many	center	182	80	140	197
	model's choice	85	94	83	117
one at a time	center	129	140	131	206
	model's choice	99	106	87	159

Table 3: Table showing counts of the first Gaussian process model had the lowest cumulative regret on a surface for the single objective Bayesian optimization experiments. The counts are the number of times a Gaussian process model did the best on a competitor for each seed. If two Gaussian process models performed the same for a given instance, they are both counted. This is for 16 competitors and 25 random seeds.

learning scenario	starting point	MOGP	Avg GP	LMC	LVMOGP
learning many	center	3.13	3.25	3.11	2.58
	model's choice	3.08	2.63	3.09	2.44
one at a time	center	2.94	3.06	2.85	2.15
	model's choice	2.94	2.63	2.63	1.81

Table 4: Table showing the mean number of iterations need for the models to get within tolerance of the target rate (± 0.05) for the single objective optimization. This is for 16 competitors and 25 random seeds.

8.4.2 Bayesian Optimization with Drift Penalty

Extra results for the Bayesian optimization with a penalty on drift. These results demonstrate that the LVMOGP gets to the best point more often (Table 5) and has the lowest cumulative regret (Table 6) more often than the other models for most of the learning scenarios. The LVMOGP also reaches the best point in the lowest number of iterations for all the learning scenarios (Table 7).

learning scenario	starting point	MOGP	Avg GP	LMC	LVMOGP
learning many	center	142	157	123	165
	model's choice	89	122	101	111
one at a time	center	141	137	153	217
	model's choice	75	102	79	164

Table 5: Table showing counts of the first Gaussian process model to reach the best point on a surface for the penalized Bayesian optimization experiments. The counts are the number of times a Gaussian process model did the best on a competitor for each seed. If two Gaussian process models performed the same for a given instance, they are both counted. This is for 16 competitors and 24 random seeds.

learning scenario	starting point	MOGP	Avg GP	LMC	LVMOGP
learning many	center	180	118	100	163
	model's choice	85	103	84	111
one at a time	center	173	118	139	204
	model's choice	83	70	65	156

Table 6: Table showing counts of the first Gaussian process model had the lowest cumulative regret on a surface for the penalized Bayesian optimization experiments. The counts are the number of times a Gaussian process model did the best on a competitor for each seed. If two Gaussian process models performed the same for a given instance, they are both counted. This is for 16 competitors and 24 random seeds.

learning scenario	starting point	MOGP	Avg GP	LMC	LVMOGP
learning many	center	2.47	3.26	2.95	2.38
	model's choice	3.39	3.13	3.23	2.13
one at a time	center	3.00	3.20	2.82	2.47
	model's choice	2.70	2.69	2.44	1.41

Table 7: Table showing the mean number of iterations need for the models to either get within tolerance of the target rate (± 0.05) without drift penalty or reach the best point (which may have a penalty) for the penalized optimization. For some runs, one or more of the models would not achieve this within the experimental budget. In these cases, the affected competitors were removed and the mean taken of the remaining. This is for 16 competitors and 24 random seeds.

8.4.3 Comparison of Choice of First Point

Table 8 shows the average regret of the first data point chosen by each of the models for each of the learning scenarios. From this table, it is clear to see the AvgGP and the LVMOGP improve on the regret of the central point, and outperform the random selection of the MOGP and LMC. This demonstrates that having a principled method of selecting the first point is useful for reducing regret.

learning scenario	starting point	MOGP	Avg GP	LMC	LVMOGP
learning many	center	0.588	0.588	0.588	0.588
	model's choice	0.651	0.499	0.703	0.464
one at a time	center	0.588	0.588	0.588	0.588
	model's choice	0.675	0.308	0.623	0.309

Table 8: Table of the mean regret of the first data point for each of the learning scenarios for each of the models.

8.5 Optimization of Gaussian Process Models

We used gradient descent to optimize the Gaussian process hyperparameters. The optimization of the hyperparameters of the Gaussian process models are non-convex problems, meaning gradient descent algorithms will only find local optima. To improve the hyperparameter optimization procedure, we used principled methods of initialization along side random restarts to fit the same Gaussian process model multiple times, and then select the hyperparameter configuration with the best log marginal likelihood. These regimes differ slightly for the different models.

For all model, unless otherwise states, we initialize the lengthscale randomly as $\ell \sim \text{Uniform}(0, 1)$, noise variance randomly as $\sigma_n \sim \text{Uniform}(0, 0.1)$ and kernel variance $\sigma_k = 1$. For the MOGP and AvgGP we did nine random restarts with these settings.

For the LMC we used three different methods for initializing \mathbf{W} and $\boldsymbol{\kappa}$, with three random restarts for each:

- *Both \mathbf{W} and $\boldsymbol{\kappa}$ random.* In this initialization, we initialize $\mathbf{W} \sim \text{Uniform}(0.1, 1)$ and $\boldsymbol{\kappa} \sim \text{Uniform}(0.1, 1)$.
- *\mathbf{W} random and $\boldsymbol{\kappa} = 0$.* In this initialization $\mathbf{W} \sim \text{Uniform}(0.1, 1)$ and $\boldsymbol{\kappa} = 10^{-6}$. This initialization was chosen as we thought it would favor solutions with small $\boldsymbol{\kappa}$ so it would better fit the linear correlation case, where the test functions are generated as linear combinations of some linear functions.
- *\mathbf{W} random and $\boldsymbol{\kappa} = 1$.* In this initialization $\mathbf{W} \sim \text{Uniform}(0.1, 1)$ and $\boldsymbol{\kappa} = 1$. We chose this initialization to favor large $\boldsymbol{\kappa}$, which is useful for the uncorrelated test case, as it would encourage the output functions to behave independently of each other.

The random initialisations for \mathbf{W} helped the initialisations for two reasons: firstly, in the GPflow implementation if \mathbf{W} is not initialized it defaults to a rank of 1, and secondly by initializing to random values rather than all one value we avoid saddle points on the optimization surface.

For the LVMOGP we used three different initialization procedures, again with three random restarts for each:

- *Random.* In this initialization all hyperparameters and variational parameters were initialized randomly. the means of the latent variables were initialized as $\mu_H \sim \text{Uniform}(-1, 1)$.
- *GPy.* This is the method used in the GPy implementation of the LVMOGP (Dai et al., 2017), that has following three steps:
 1. A sparse MOGP is fitted to the data using a set of inducing points Z which are common to all outputs. The mean predictions $\mu(Z) \in \mathbb{R}^{N_U \times P}$ of the output function values at these inducing inputs is then calculated:

$$\mu(Z) = K(Z, Z)[K(Z, Z) + \sigma_n^2 \mathbf{I}]^{-1} Y. \quad (20)$$

The sparse MOGP is used to ensure all output functions are observed at the same input locations for the functional PCA, which is necessary when data is observed at different locations on different surfaces. It also serves the purpose of smoothing the data plus the trained lengthscales are used to initialise the lengthscales of the observed dimensions of the LVMOGP.

2. The mean predictions $\mu(Z) \in \mathbb{R}^{N_U \times P}$ are then used as inputs to functional PCA. The first Q_H eigenvectors $V \in \mathbb{R}^{N_U \times Q_H}$ and eigenvalues $\{\lambda_q\}_{q=1}^{Q_H}$ of $\mu(Z)^T \mu(Z)$ are calculated and used to project $\mu(Z)$ into latent space

$$H = \mu(Z)^T V, \quad (21)$$

where $H \in \mathbb{R}^{P \times Q_H}$. The relative contributions of each of the eigenvalues is also calculated as:

$$s_q = \frac{\tilde{\lambda}_q}{\max\{\tilde{\lambda}_i\}_{i=1}^{Q_H}} \quad \tilde{\lambda}_q = \frac{\lambda_q}{\sum_{i=1}^{Q_H} \lambda_i} \quad (22)$$

3. The latent variables H from the functional PCA are used to initialize the latent variables of a Bayesian Gaussian process latent variable model. The lengthscales of the Bayesian Gaussian process latent variable model are initialized to $\{\frac{1}{s_q}\}_{q=1}^{Q_H}$. Once the Bayesian Gaussian process latent variable model is trained, the latent variables and hyperparameters of the Bayesian Gaussian process latent variable model are used to initialize those of the LVMOGP.
- *PCA*. In this initialization, the first two steps of the *GPy* initialization are followed. This means fitting a sparse MOGP to the data and performing principle component analysis (PCA) on the posterior predictions at inducing point locations. The MOGP hyperparameters were then used to initialize the LVMOGP observed lengthscale, kernel variance and noise variance. The output of the PCA was used to initialize the latent variable means and the lengthscale of the latent dimensions. This initialization was chosen as a simplified version of the *GPy* initialization.

See the github repositories in Appendix 8.2 for more details.

In the synthetic experiments, we found the method of initializing the hyperparameters affected the end log marginal likelihood, with no initialization outperforming all others for each model. Therefore, we decided to continue with all initializations for the PCR data experiments. For the PCR data experiments we did 10 random restarts for each initialization, due to the randomness of some of the initializations.